

LARGE-SCALE ENVIRONMENTAL DEPENDENCE OF GAS-PHASE METALLICITY IN DWARF GALAXIES

KELLY A. DOUGLASS, MICHAEL S. VOGLEY

Department of Physics, Drexel University, 3141 Chestnut Street, Philadelphia, PA 19104

ABSTRACT

We study how the cosmic environment affects galaxy evolution in the Universe by comparing the metallicities of dwarf galaxies in voids with dwarf galaxies in more dense regions. Ratios of the fluxes of emission lines, particularly those of the forbidden [O III] and [S II] transitions, provide estimates of a region’s electron temperature and number density. From these two quantities and the emission line fluxes [O II] λ 3727, [O III] λ 4363, and [O III] $\lambda\lambda$ 4959, 5007, we estimate the abundance of oxygen with the Direct T_e method. We estimate the metallicity of 37 void dwarf galaxies and 75 dwarf galaxies in more dense regions using spectroscopic observations from the Sloan Digital Sky Survey Data Release 7, as re-processed in the MPA-JHU value-added catalog. We find very little difference between the two sets of galaxies, indicating little influence from the large-scale environment on their chemical evolution. Of particular interest are a number of extremely metal-poor dwarf galaxies that are equally abundant in both voids and denser regions.

Keywords: galaxies: abundances — galaxies: dwarf — galaxies: evolution

1. INTRODUCTION

Galaxy redshift surveys have shown that the large-scale structure of the galaxy distribution is similar to that of a three-dimensional cosmic web (Bond et al. 1996) in which the voids (large, underdense regions that fill upwards of 60% of space) separate galaxy clusters connected by thin filaments of galaxies. The voids found in early surveys (e.g., Gregory & Thompson 1978; Kirshner et al. 1981; de Lapparent et al. 1986) proved to be an ubiquitous feature of large-scale structure. Analyses of the Sloan Digital Sky Survey (Abazajian et al. 2009; Ahn et al. 2012) have yielded catalogs of 10^3 voids (Pan et al. 2012; Sutter et al. 2014).

These cosmic voids are an important environment for studying galaxy formation (see van de Weygaert & Platen (2011) for a review). The Λ CDM cosmology predicts that galaxies formed in voids should have lower mass and be retarded in their evolution when compared to those in more dense environments (e.g., Gottlöber et al. 2003; Goldberg et al. 2005; Cen 2011). Gravitational clustering within a void proceeds as if in a very low density universe, in which structure formation occurs early and there is relatively little interaction between galaxies, both because of the lower density and the faster local Hubble expansion.

Goldberg & Vogeley (2004) show that the interior of a spherical void with 10% of the mean density in a $\Omega_{matter} = 0.3$, $h = 0.7$ universe evolves dynamically like an $\Omega_{matter} = 0.02$, $\Omega_{\Lambda} = 0.48$, $h = 0.84$ universe. Hydrodynamical cosmological simulations by Cen (2011) show that the gas in voids remains below the critical entropy threshold, allowing the void galaxies to continue forming stars. While the more dense environment of cluster galaxies drastically alters their chemical composition and future evolution through the relatively frequent occurrences of mergers, tidal stripping, and/or ram-pressure stripping, void galaxies evolve in a relatively pristine environment where interactions are far less frequent and star formation may proceed up to the present epoch because void galaxies are able to retain their gas.

The effects of the void environment should be most obvious in the dwarf galaxies. Dwarf galaxies are sensitive to many astrophysical effects, including cosmological reionization, internal feedback from supernova and photoheating from star formation, external effects from tidal interactions and ram pressure stripping, small-scale details of dark matter halo assembly, and properties of dark matter. Many of these effects have been invoked to attempt to resolve the discrepancy between the mass function of galaxy halos predicted by Λ CDM and the observed, much smaller density of dwarf galaxies observed in voids (see, e.g., Kravtsov (2009) for a review). It is critical to explore dwarfs in voids to complement studies of dwarfs in groups and clusters because the assem-

bly histories of low-mass galaxies are predicted to be very different (e.g., Gao & White 2007; Lackner et al. 2012) and observations to date show that the properties of dwarfs vary dramatically with environment (e.g., Ann et al. 2008; Geha et al. 2012). Diffuse cold-mode accretion, rather than mergers, has been suggested to be the dominant mechanism for growing dark matter halos in voids (e.g., Kereš et al. 2005; Fakhouri & Ma 2009). Late-time gas accretion may be possible in voids if void galaxies retain a baryonic reservoir up to the present epoch. Thus, these few, lonely, faint galaxies test important features of the structure formation model and our understanding of galaxy formation “gastrophysics.”

Observational studies of void galaxies have included examination of photometric properties such as luminosity (Hoyle et al. 2005; Croton et al. 2005; Moorman et al. 2015), color and morphological type (Grogin & Geller 2000; Rojas et al. 2004; Patiri et al. 2006; Park et al. 2007; von Benda-Beckmann & Müller 2008; Hoyle et al. 2012) star formation rates estimated from optical spectroscopy and UV photometry (Rojas et al. 2005; Moorman et al. 2015; Beygu et al. 2016), and gas content (Kreckel et al. 2012; Moorman et al. 2016; Jones et al. 2016). Void galaxies tend to be of lower luminosity, of late morphological type, blue, have relatively high rates of star formation per stellar mass, and gas rich.

Another important test of galaxy formation is metallicity, which is a measure of the integrated star formation history and is frequently characterized by the ratio of the oxygen to hydrogen atomic density (often $Z = 12 + \log(\text{O}/\text{H})$, though sometimes given in units of the solar metallicity, Z/Z_{\odot}). The metallicity should depend on the galaxy’s formation history, specifically the percentage of its gas that has been turned into stars (Guseva et al. 2009). If void galaxies have only recently started forming stars, have been forming stars at a low rate through time, or have recently accreted unprocessed gas, we would expect these galaxies to have a lower metallicity than those in more dense regions (whose star formation started earlier and/or has been at a much higher rate, due to e.g., tidally-triggered star formation). Furthermore, gas-phase metallicity is affected by the evolution of a galaxy’s stellar population and the composition of its interstellar medium (ISM). It reveals a galaxy’s history of releasing metals into the ISM via supernovae and stellar winds, ejecting gas via galactic outflows, and accreting gas from the surrounding environment (see, e.g., Cooper et al. 2008; Cybulski et al. 2014; Hirschmann et al. 2014, and references therein). Understanding the evolution of metallicity in galaxies is therefore crucial in uncovering the details of galactic evolution.

Observations by Cooper et al. (2008); Deng (2011);

Filho et al. (2015); Pustilnik et al. (2006, 2011b,a); Pustilnik et al. (2013); Pustilnik (2014) appear to support the hypothesis of lower metallicity in void galaxies, while Kreckel et al. (2015) find no effect of the void environment on their sample of eight void dwarf galaxies. Most of the conclusions of previous work are based on samples containing only a handful of galaxies. Because large sky surveys like SDSS contain a substantial collection of dwarf galaxies, we can now analyze the dwarf galaxy population in the relatively nearby universe to test this hypothesis with more statistical significance. In particular, the main galaxy sample of SDSS DR7 covers a large enough volume to identify over 1000 voids (Pan et al. 2012) and provides spectroscopy to permit metallicity estimates of void dwarf galaxies. We make use of the reprocessed spectroscopic data from the MPA-JHU catalog¹ to study the metallicity of the large collection of dwarf galaxies in SDSS DR7. As explained by Tremonti et al. (2004), the spectra in the MPA-JHU catalog are analyzed with a more detailed stellar continuum, permitting the weaker emission lines to become more apparent. With the dependence of our analysis on weak emission lines (especially [O III] $\lambda 4363$), this detailed treatment of the weak emission lines should produce more accurate results. We study the metallicity of these galaxies as a function of large-scale environment, testing the hypothesis that void dwarf galaxies have lower gas-phase metallicities than dwarf galaxies in more dense regions.

Our paper is organized as follows. Section 2 describes the theory behind using various emission lines to estimate the metallicity of galaxies. We review the source of our data in Section 3. An overview of the metallicity method calculations and sources of error is included in Section 4. Section 5 discusses the results of our metallicity calculations and their implication on the large-scale environmental influence. Finally, Section 6 summarizes our conclusions and discusses future work.

2. ESTIMATION OF GALAXY METALLICITY FROM OPTICAL SPECTROSCOPY

2.1. Overview of Methods

We characterize the galaxy metallicity using oxygen because it is relatively abundant, it emits strong lines for several ionization states in the optical regime, and a ratio of its lines provides a good estimate of the electron temperature (Kewley & Dopita 2002). Here, we describe the theory and method we employ to estimate oxygen abundances in dwarf galaxies.

UV photons from young stars in an H II region

¹ Available at <http://www.mpa-garching.mpg.de/SDSS/DR7/>

keep the interstellar gas partially ionized. Optical photons are either absorbed and re-emitted throughout the region at resonant frequencies (resulting in classically permitted electron transitions), or the electrons are collisionally excited (resulting in classically forbidden electron transitions). Collisional excitation of the lower energy levels of metal ions is possible because these levels are only a few eV above the ground state (De Robertis et al. 1987). Consequently, the UV-optical spectrum contains some of the most useful diagnostic emission lines. Due to observational constraints of SDSS DR7 (the spectrometer’s wavelength range and the signal-to-noise of the resulting spectra; see Section 3), not all these emission lines are easily measured.

Three classes of methods have been developed to estimate the gas-phase metallicity of a galaxy, which we label as direct, theoretical, and empirical. Direct- T_e methods are based on a measurement of the [O III] $\lambda 4363$ auroral line, from which a “direct” estimate of the electron temperature can be made (e.g., Izotov et al. 2006; Kniazev et al. 2008; Pilyugin & Thuan 2007; Yin et al. 2007). Theoretical methods are based on photoionization models (e.g., Kewley & Dopita 2002). Empirical methods make an indirect estimate of the electron temperature based on calibrated relationships between direct metallicity estimates and other strong-line ratios in H II regions (see, for example, Pettini & Pagel 2004; Pilyugin & Mattsson 2011; Dopita et al. 2013; Lara-Lopez et al. 2013; Marino et al. 2013). While each of these methods provides an estimate for the metallicity, they are all developed for use on sets of galaxies with different characteristics (stellar mass or gas-phase metallicity, for example). Previously, most theoretical and empirical methods have been calibrated with galaxies of larger stellar mass and higher luminosity. Due to the differing properties of dwarf galaxies from those of higher luminosity (and larger stellar mass), most of these methods drastically over- or under-estimate the gas-phase metallicity for dwarf galaxies. Consequently, we must exercise caution when applying these various calculation methods for estimating the metallicity of dwarf galaxies. We attempt to avoid any calibration issues by estimating gas-phase metallicity using the direct- T_e method. This method relies on the weak [O III] $\lambda 4363$ emission line, which limits the number of dwarf galaxies we can analyze. However, because this method provides more reliable metallicity estimates than any of the others for dwarf galaxies, we chose quality over quantity in our results.

2.2. [O III]

There are three significant emission lines for doubly-ionized oxygen. The relative excitation rates to the 1S and 1D energy levels depend very strongly on the elec-

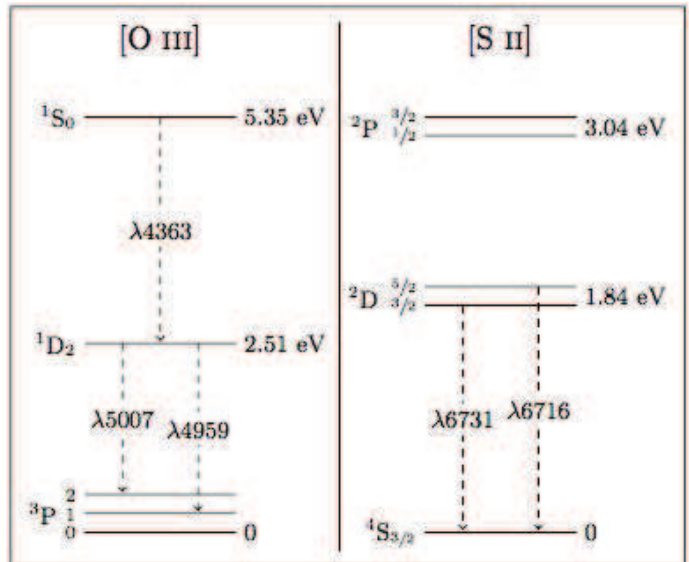


Figure 1. Energy-level diagram for [O III] ($2p^2$) and [S II] ($3p^3$) ions. The most important transitions are shown; all are in the visible spectrum. These forbidden transitions in oxygen provide an estimate of the electron temperature in the interstellar gas, while the forbidden sulfur transitions provide an estimate of the electron number density. With estimates of the electron temperature and number density, we can convert emission line flux ratios into chemical abundance ratios.

tron temperature, T_e ; therefore, the relative strengths of these emitted lines can be used to measure the electron temperature (Osterbrock 1989). In the low-density limit ($n_e < 10^5 \text{ cm}^{-3}$), most excitations to the 1D level result in an emission of a photon with a wavelength of either 5007\AA or 4959\AA , as shown in Fig. 1. Most excitations up to 1S produces a photon of wavelength 4363\AA , followed by a photon of either of the two previous wavelengths (since the electron is now in the 1D level).

At higher densities, collisional de-excitation begins to influence these emission rates (Osterbrock 1989). Because the 1D level has a longer lifetime than the 1S state, it is collisionally de-excited at lower electron densities. This weakens the $\lambda 4959$ and $\lambda 5007$ emission lines. At the same time, the additional collisional excitations of the 1D state permitted by the higher electron densities strengthens the $\lambda 4363$ emission line.

[O III] $\lambda 4363$ is a temperature-sensitive forbidden transition line of doubly-ionized oxygen that is the preferred line to use when measuring the metallicity of galaxies. Since the most effective cooling channel in these H II regions is oxygen line emission, lower metallicities correspond to higher temperatures (Saintonge 2007). Because collisional de-excitations (which reduce the number of transitions at this level) become more frequent at higher temperatures (higher chemical abundances), its strength is inversely proportional to the metallicity of a galaxy. [O III] $\lambda 4363$ is already one

to two orders of magnitude weaker than the [O III] $\lambda\lambda 4959, 5007$ doublet, so it is very difficult to obtain an accurate ratio with this line. It is for these reasons that other “empirical” relations were developed for metallicity calculations, eliminating the need of an electron temperature estimate from this emission line.

Given an electron temperature and density, the flux ratio of the [O III] $\lambda\lambda 4959, 5007$ doublet to $H\beta$ provides an abundance estimate for doubly-ionized oxygen.

2.3. [O II]

A less temperature-sensitive line than [O III] $\lambda 4363$, the [O II] $\lambda 3727$ forbidden transition doublet of singly-ionized oxygen is often used in metallicity calculations. With an electron temperature and density, its flux provides an estimate of the abundance of singly-ionized oxygen. In SDSS spectra, this line can be observed for objects with a redshift greater than 0.02. However, because dwarf galaxies are inherently faint objects ($M_r > -17$), they are targeted for spectroscopy in SDSS only out to redshift $z \sim 0.03$, thus we can only estimate the metallicity of dwarf galaxies in the redshift range $0.02 < z < 0.03$.

2.4. [S II]

Just as we are able to measure the electron temperature from [O III] transitions, we can estimate the electron number density from [S II] transitions. Below a density of about 100 cm^{-3} , the [S II] $\lambda 6716/\lambda 6731$ ratio has a weak dependence on the density. All our galaxies fall within this low-density regime, so we assume a low-density limit of $n_e = 100 \text{ cm}^{-3}$.

2.5. Direct T_e method

We use the method published by [Izotov et al. \(2006\)](#), which is based on the astrophysics in [Osterbrock \(1989\)](#). It makes use of the [O III] $\lambda 4363, \lambda\lambda 4959, 5007$ lines and the [O II] $\lambda 3727$ doublet. While often regarded as the most accurate estimate of the metallicity, it is difficult to employ due to the restrictions on [O III] $\lambda 4363$. Consequently, this method is best suited for low-redshift, low-metallicity galaxies. The electron temperature is derived by solving the following system of equations:

$$t_3 = \frac{1.432}{\log[(\lambda 4959 + \lambda 5007)/\lambda 4363] - \log C_T} \quad (1)$$

where $t_3 = 10^{-4}T_e(\text{O III})$ and

$$C_T = (8.44 - 1.09t_3 + 0.5t_3^2 - 0.08t_3^3) \frac{1 + 0.0004x_3}{1 + 0.044x_3} \quad (2)$$

where $x_3 = 10^{-4}n_e t_3^{-0.5}$. The ionic abundances are then found with the equations

$$12 + \log\left(\frac{\text{O}^+}{\text{H}^+}\right) = \log\frac{\lambda 3727}{H\beta} + 5.961 + \frac{1.676}{t_2} - 0.40 \log t_2 - 0.034t_2 + \log(1 + 1.35x_2) \quad (3)$$

$$12 + \log\left(\frac{\text{O}^{++}}{\text{H}^+}\right) = \log\frac{\lambda 4959 + \lambda 5007}{H\beta} + 6.200 + \frac{1.251}{t_3} - 0.55 \log t_3 - 0.014t_3 \quad (4)$$

where $t_2 = 10^{-4}T_e(\text{O II})$, $T_e(\text{O II}) = 0.7T_e(\text{O III}) + 0.3$ ([Garnett 1992](#)), and $x_2 = 10^{-4}n_e t_2^{-0.5}$. [Andrews & Martini \(2013\)](#) have shown that this relation between $T_e(\text{O II})$ and $T_e(\text{O III})$ may overestimate the temperature in the low ionization zone, causing the calculated metallicities to be underestimated. Because we care only about the relative metallicity values of the galaxies, this effect does not affect our conclusions.

The total gas-phase oxygen abundance is equal to the sum of the abundances of each of the ionized populations:

$$\frac{\text{O}}{\text{H}} = \frac{\text{O}^+}{\text{H}^+} + \frac{\text{O}^{++}}{\text{H}^+} \quad (5)$$

3. SDSS DATA AND GALAXY SELECTION SAMPLE

The SDSS Data Release 7 (DR7) ([Abazajian et al. 2009](#)) is a wide-field multi-band imaging and spectroscopic survey, using drift scanning to map approximately one-quarter of the northern sky. Photometric data in the five band SDSS system — $u, g, r, i,$ and z — are taken with a dedicated 2.5-meter telescope at the Apache Point Observatory in New Mexico ([Fukugita et al. 1996](#); [Gunn et al. 1998](#)). Galaxies with a Petrosian r -band magnitude $m_r < 17.77$ are selected for spectroscopic analysis ([Lupton et al. 2001](#); [Strauss et al. 2002](#)). The spectra have an observed wavelength range of 3800\AA to 9200\AA with a resolution $\lambda/\Delta\lambda \sim 1800$, and are taken using two double fiber-fed spectrographs and fiber plug plates with a minimum fiber separation of 55 arcseconds ([Blanton et al. 2003](#)). The emission line flux data used in this study are from the MPA-JHU value-added catalog, which is based on the SDSS DR7 sample of galaxies. Absolute magnitudes, colors, and all other additional data are from the KIAS value-added galaxy catalog ([Choi et al. 2010](#)).

3.1. Spectroscopic selection

To satisfy the needs of our analysis, we make the following cuts to our sample. All analyzed galaxies must

have relatively recent star formation, since UV photons are needed to excite the interstellar gas to produce the required emission lines. In addition, because we analyze only dwarf galaxies ($M_r > -17$), there is a natural redshift upper limit of 0.03 on the samples; dwarf galaxies at higher redshifts are not bright enough to be included in the spectroscopic data of SDSS. For a galaxy to be analyzed, we require a minimum 5σ detection of the $H\beta$ emission line and at least a 1σ detection of the [O III] $\lambda 4363$ forbidden transition. The restriction on both these lines eliminate those galaxies with a low S/N spectrum. This is particularly important for [O III] $\lambda 4363$, as it is inherently a weak emission line. We are aware that implementing this restriction on [O III] $\lambda 4363$ eliminates those galaxies with higher metallicities, since the strength of this line is inversely proportional to the metallicity of the galaxy (see Sec. 2.2 for details). However, we show that this restriction does not affect our conclusions on the large-scale environmental dependence on the gas-phase metallicity.

In addition, we also eliminate galaxies with both [O III] $\lambda 4959/H\beta < 0.7$ and [O II] $\lambda 3727/H\beta > 1.0$, following the restrictions used by Izotov et al. (2006). This removes galaxies in which a significant enhancement of the weak [O III] $\lambda 4363$ emission line from the H II region may be due to a different mechanism than photoionization heating. The additional restriction on the [O II] $\lambda 3727$ line (relative to $H\beta$) ensures that we do not eliminate galaxies with more metal-deficient high-excitation H II regions.

For the dwarf galaxies in our sample, the [O II] $\lambda 3727$ spectral line is very close to the edge of the spectrometer due to their maximum redshift $z < 0.03$. Consequently, its flux measurement is not always reliable. Therefore, the flux values labeled `oii_flux` in the MPA-JHU catalog are used instead of the combined flux values measured for the [O II] $\lambda\lambda 3726, 3729$ doublet. Because the velocity dispersion is not fixed when measuring the flux found in `oii_flux`, the resulting measurements tend to be more realistic than those measured with the fixed dispersion (C. Tremonti, private communication). In addition, those galaxies with remaining erroneous measurements for the [O II] $\lambda 3727$ doublet were removed by hand, after comparing the listed flux values to the spectra by eye. All spectral lines used in the analysis must have a flux greater than 0, to ensure that they are emission lines.

3.2. Void classification

Void galaxies are identified using the void catalog compiled by Pan et al. (2012), which was built based on the galaxies in SDSS DR7 catalog. Starting with galaxies with absolute magnitudes $M_r < -20$, the VoidFinder algorithm of Hoyle & Vogeley (2002) removes all isolated

galaxies (defined as having the third nearest neighbor more than $7 h^{-1}$ Mpc away). After applying a grid to the remaining galaxies, spheres are grown from all empty grid cells (cells containing no galaxies). A sphere reaches its maximum size when it encounters four galaxies on its surface. To be classified as a void (or part of one), a sphere must have a minimum 10 Mpc radius. If two spheres overlap by more than 10%, they are considered part of the same void. See Hoyle & Vogeley (2002) for a more detailed description of the VoidFinder algorithm. Those galaxies that fall within these void spheres are classified as void galaxies. Those galaxies that lie outside the spheres are classified as wall galaxies. Because we cannot identify any voids within 10 Mpc of the edge of the survey, we do not include the galaxies that fall within this region in either the void or wall sample (throughout this paper, these galaxies are labeled as “Uncertain”).

Of the $\sim 800,000$ galaxies with spectra available in SDSS DR7, 9519 are dwarf galaxies. Applying the spectroscopic cuts, 37 void dwarf galaxies and 75 wall dwarf galaxies are left to analyze.

4. METALLICITY ANALYSIS AND RESULTS

Our primary objective is to perform a relative measurement of metallicity of dwarf galaxies to discern how the large-scale environment affects their chemical evolution. As discussed in Section 2, the strength of and ability to observe different spectral lines between various surveys and observations require multiple methods to be developed for metallicity calculations. In this paper, we use only the Direct T_e method, because no other method has yet been calibrated using dwarf galaxies. The results from the various methods are not directly comparable; while they all return metallicities within the same range, the same galaxy can have very different metallicity values depending on which method is used. Conversions between methods have been developed (see Kewley & Ellison 2008), but it is not clear that these conversions would be accurate for dwarf galaxies. Unfortunately, there are not enough galaxies available in our sample to calibrate these other methods for dwarf galaxies.

All line ratios listed are ratios of the emission line fluxes. Galaxies with low metallicities have $Z = 12 + \log(\text{O}/\text{H}) < 7.6$ (Pustilnik et al. 2006); galaxies with high metallicities have $Z > 8.2$ (Pilyugin et al. 2006). The solar metallicity $Z_{\odot} = 8.86$ (Delahaye & Pinsonneault 2006).

4.1. Estimation of uncertainties and confirmation of our method

We estimate uncertainties in the computed metallicity using a Monte-Carlo method. Using the measured

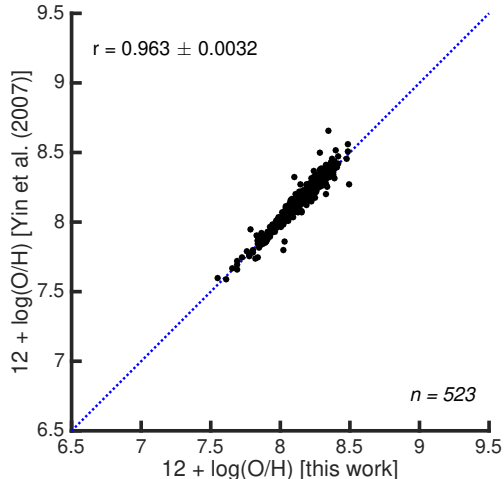


Figure 2. Metallicity ($12 + \log(\text{O}/\text{H})$) comparison between our calculated estimates and those made by Yin et al. (2007). Error bars have been omitted for clarity. The axes limits here match the metallicity range used throughout the remainder of this paper. These are not the dwarf galaxies analyzed in this paper, but rather the sample of galaxies analyzed by Yin et al. (2007) to confirm that our version of the calculation is correct. Both Yin et al. (2007) and we have used the metallicity method outlined by Izotov et al. (2006).

line fluxes and corresponding errors from the MPA-JHU catalog, 100,000 different metallicities are calculated for a given galaxy. For each estimate, the flux of a line is drawn from a normal distribution, with the expectation value being the original measured flux and the standard deviation being the given error in the flux measurement. The standard deviation in the set of these 100,000 calculated values is used as the error in the metallicity estimate for the galaxy. As a result, these uncertainties tend to be larger than those quoted in other sources, as they include more information than just the quality of the fit used to derive the metallicity.

We compare results of our analysis of the same set of SDSS galaxies that Yin et al. (2007) analyzed to confirm that our code was working properly, since Yin et al. (2007) also uses the metallicity method outlined in Izotov et al. (2006). The results of this comparison can be seen in Fig. 2. Yin et al. (2007) also used the MPA-JHU catalog as the source for their data, so our results should be identical.

4.2. Results

Metallicities calculated using the Direct T_e method for our dwarf galaxy sample are listed in Table A1, along with other key identification for the galaxies (including whether they are a void or wall galaxy). A histogram of the resulting metallicities is shown in Fig. 3. As can be seen in Fig. 3, there is very little difference in the spread of metallicity values in dwarf galaxies between voids and walls. A two-sample Kolmogorov-Smirnov

(KS) test quantifies this observation — it produced a test statistic of 0.0782, corresponding to a probability of 99.7% that a test statistic greater than or equal to that observed will be measured; the cumulative distribution function (CDF) of these samples can be seen on the right in Fig. 3.

The requirement of a minimum 1σ detection of [O III] $\lambda 4363$ eliminates galaxies with a low-quality spectrum and those with a weak [O III] $\lambda 4363$ line. Since this line is inversely proportional to the oxygen abundance in the interstellar gas, this biases the sample towards more low-metallicity galaxies. To see how much this cut affects the results, we perform the same analysis with no minimum detection limit of [O III] $\lambda 4363$. As can be seen in Fig. 4, this adds a substantial number of galaxies to the sample (there are now 64 void galaxies and 120 wall galaxies analyzed), but there is still no difference between the percentages of low metallicity galaxies and high metallicity galaxies in the voids and walls: see Table 1 for details. Indeed, the two-sample KS test returned a test statistic of 0.1052, corresponding to a probability of 72% that a larger test statistic will be seen; the CDF of these samples can be seen in Fig. 4. Thus, there is no evidence for a significant difference in the metallicity values of void and wall dwarf galaxies.

Table 1. Metallicity population percentages

	$Z < 7.6$	$7.6 \leq Z < 8.2$	$Z \geq 8.2$
1σ restriction on [O III] $\lambda 4363$			
Void	8.11% (3)	64.86% (24)	27.03% (10)
Wall	9.33% (7)	65.33% (49)	25.33% (19)
No restriction on [O III] $\lambda 4363$			
Void	7.81% (5)	51.56% (33)	40.62% (26)
Wall	12.50% (15)	50.00% (60)	37.50% (45)

NOTE—Percentages of galaxies with calculated metallicities within the labeled metallicity ranges, with the number of galaxies in each category in parentheses. Even with the additional galaxies with no restriction, there is still very little large-scale environmental dependence on the metallicity of dwarf galaxies.

4.3. Sources of systematic error

It is well-known that many physical properties of galaxies vary with the distance from the center of the galaxy (Bell & de Jong 2000). Therefore, a metallicity

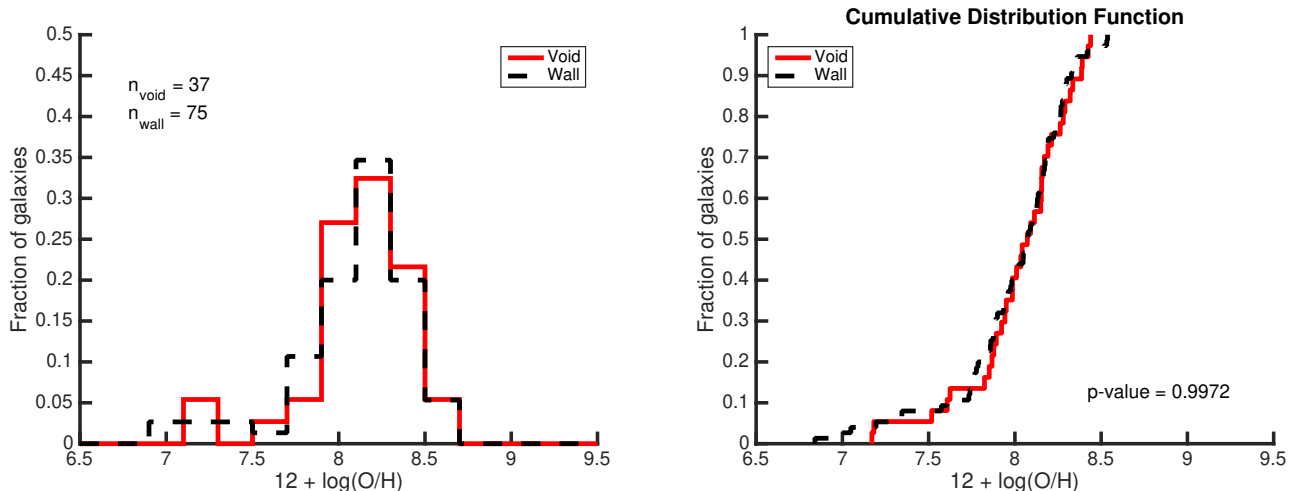


Figure 3. Histogram and associated cumulative distribution function of the gas-phase metallicity of void dwarf (red dashed line) and wall dwarf (black solid line) galaxies. A two-sample KS test of the two data sets results in an asymptotic p -value of 0.9972, indicating a 99.7% probability that a test statistic greater than the observed value of 0.0782 will be seen. This is reflected visually, as there appears to be very little difference in the two populations, indicating that there is little large-scale environmental influence on the metallicity of dwarf galaxies.

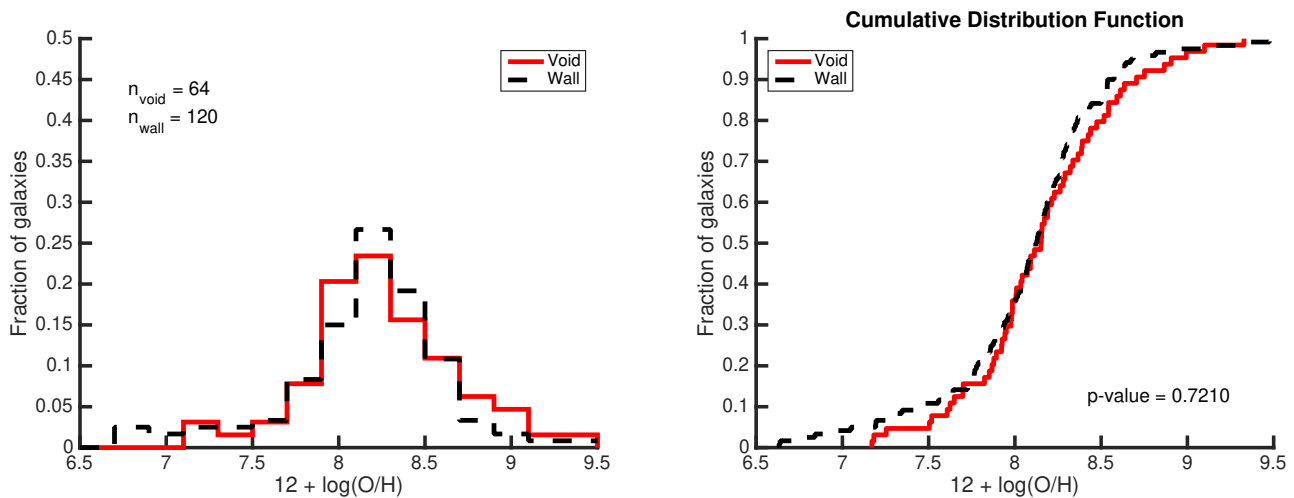


Figure 4. Histogram and associated cumulative distribution function comparing the gas-phase metallicity of void dwarf (red dashed line) and wall dwarf (black solid line) galaxies. The galaxies here have no minimum detection of the auroral $[\text{O III}] \lambda 4363$ line. As expected, eliminating the restriction on this line includes more high metallicity galaxies to the sample, but there is still no significant difference between the void and wall galaxies – a two-sample KS test here produced a p -value of 0.7210.

measurement is dependent on the location of the spectroscopic fiber on the galaxy. If not all the light of the galaxy is contained within the fiber of the spectrograph, the estimated metallicity will not necessarily be representative of a global metallicity value. Indeed, it has been shown that different parts of a galaxy have different metallicity values (Bell & de Jong 2000). In SDSS, the fiber size is 3 arcseconds – this corresponds to a physical diameter between 1.29 kpc and 1.93 kpc, at redshifts $0.02 < z < 0.03$. For many of the dwarf galaxies, this covers more than 50% of the galaxy’s luminous surface. The fiber is almost always centered on the brightest spot of the galaxy. For spiral and elliptical galaxies, this is

often the center of the galaxy. Since this is the oldest part of the galaxy, these metallicity values may be over-estimates of the global metallicity. Many dwarf galaxies are irregular galaxies, where the fiber is instead focused on a bright H II region.

Due to the requirements we place on the emission lines for the galaxies, we are inherently limiting our sample to only blue, star-forming galaxies. This is not a representative sample of the dwarf galaxy population. Rather, in this study we are only able to comment on the large-scale environmental influence on blue, star-forming dwarf galaxies in a narrow redshift range. Unfortunately, we cannot measure the metallicity of red

dwarf galaxies with the Direct T_e method, since we need the UV photons from young stars to excite the interstellar gas.

4.4. Mass-metallicity relation

A strong correlation between the stellar mass and metallicity of galaxies reflects the fundamental connection between galactic mass and the chemical evolution of galaxies. We use stellar mass estimates from the MPA-JHU catalog to examine the mass-metallicity relation in our sample of 115 dwarf galaxies. We have also included those galaxies from the MPA-JHU catalog with metallicity estimates from Tremonti et al. (2004) to place our sample in context. Due to the narrow range of masses in our sample, it is difficult to derive an accurate fit to the data. However, we make comparisons to three published mass-metallicity relations (Tremonti et al. 2004; Mannucci et al. 2010; Andrews & Martini 2013). As can be seen in Fig. 5, the relation derived by Andrews & Martini (2013) best fits the data; the fit by Mannucci et al. (2010) diverges at the low-mass limit, while the relation of Tremonti et al. (2004) predicts a higher metallicity than most measured in this sample. It is important to note that two of these relations are only calibrated down to a stellar mass of $10^{8.5} M_\odot$. In Fig. 5, these relations have been extended to $10^7 M_\odot$, in order to extend past our galaxy sample. The mass-metallicity relation derived by Andrews & Martini (2013) best fits the data because their metallicities are also derived using the Direct T_e method.

In addition to looking at the overall mass-metallicity relation for dwarf galaxies, we can also investigate the difference in the relation between galaxies in voids and those in more dense regions. There appears to be no significant differences in the two populations, indicating minimal influence from the large-scale environment on the mass-metallicity relation of these dwarf galaxies. Hughes et al. (2013) also found that the stellar mass-metallicity relation is independent of large-scale environment. This prompts the conclusion that the internal evolutionary processes of a galaxy have a greater influence on its chemical evolution than its large-scale environment. We expect this dependence of the mass of a galaxy on its chemical content, since the accumulated metals reflect the integrated history of star formation. However, we would expect an environmental dependence to appear as well, if void galaxies are in an earlier stage of evolution and/or are continuing to accrete fresh gas.

4.5. SFR-metallicity relation

A fundamental diagnostic of the star formation history of galaxies is the relation between stellar mass, metallicity, and star formation rate. Therefore, we also look

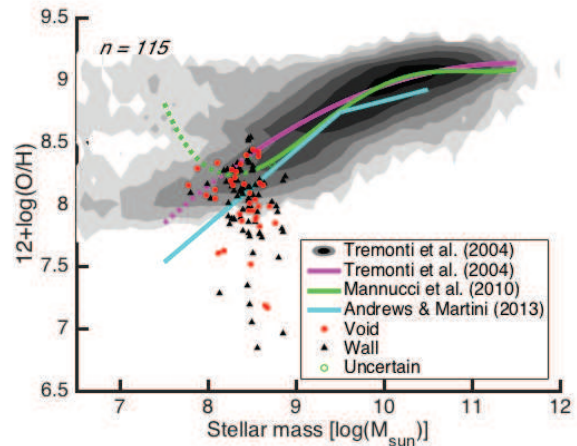


Figure 5. Stellar mass versus metallicity of the 115 analyzed dwarf galaxies. Error bars have been omitted for clarity. Due to the limited range of mass (all our galaxies are within a small range of masses, since we are looking only at dwarf galaxies), we cannot derive our own relation between the mass and metallicity. Some published relations are plotted over our data – it appears that the relation by Andrews & Martini (2013) is the most robust in the low-mass limit. To place our sample in context, we have also included (grey contours) those galaxies from the MPA-JHU catalog with metallicity estimates by Tremonti et al. (2004). It was from these galaxies that the published relation of Tremonti et al. (2004) was derived.

at the relationship between the (specific) star formation rate and metallicity of these 115 dwarf galaxies. The total (specific) star formation rate estimates for these galaxies are from the MPA-JHU value-added catalog, based on the technique discussed in Brinchmann et al. (2004). For low-mass galaxies, Henry et al. (2013) shows that the star formation rate is inversely proportional to the metallicity of a galaxy. However, this is not quite what is observed in our data, as seen in Fig. 6. The correlation coefficient between the total (specific) star formation rate and the metallicity $r_{sSFR} = 0.43 \pm 0.077$ and $r_{SFR} = 0.54 \pm 0.066$, showing a positive correlation between the two properties. Indeed, those galaxies with the lowest metallicities have some of the lowest (specific) star formation rates among the dwarf galaxies in our sample. There does not seem to be a difference between the void and wall galaxies in this relation, indicating no large-scale environmental influence on the (s)SFR–Z relation.

4.6. Color-metallicity relation

Metallicity is expected to have a positive correlation with color, as older galaxies are expected to have higher metallicities, since they have had more time to convert their gas into heavier elements through star formation. Therefore, we also look at the color–metallicity relation of our sample of 115 galaxies – these relations can be seen in Fig. 7. To place our galaxies in the context

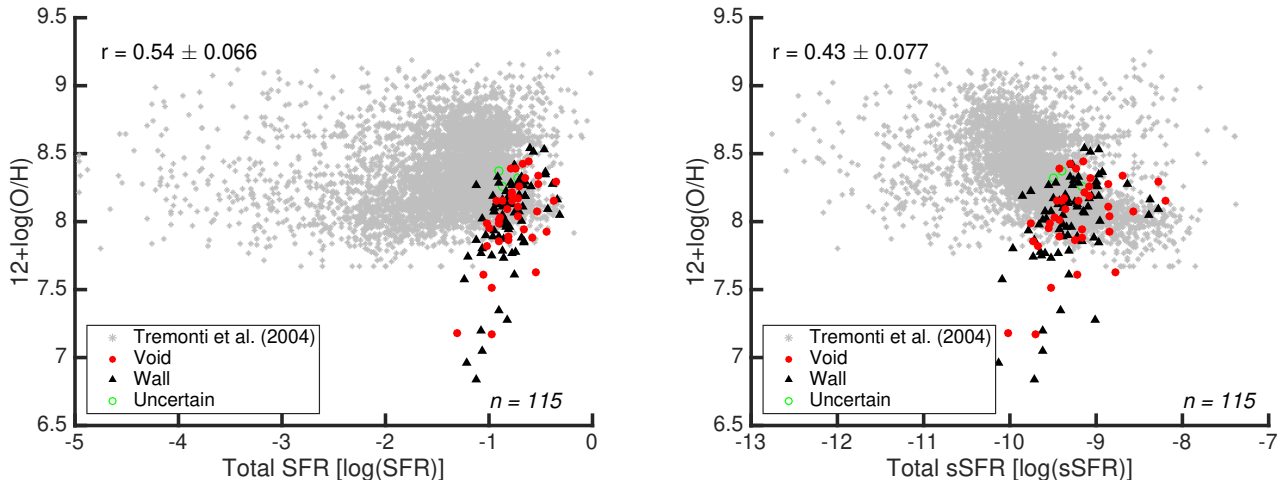


Figure 6. Total star formation rate (SFR) and specific star formation rate (sSFR) versus metallicity of the 115 analyzed dwarf galaxies. Error bars have been omitted for clarity. We also plot (grey stars) dwarf galaxies ($M_r > -17$) with metallicity estimates by Tremonti et al. (2004), to place our results in context. It is significant to note that the majority of our galaxies are on the upper end of the SFR and sSFR for dwarf galaxies. Note that those galaxies with metallicities $12 + \log(\text{O}/\text{H}) < 7.6$ are on the lower end of the range of sSFR of the dwarf galaxies in our sample.

of other dwarf galaxies, we have included the sample of dwarf galaxies for which Tremonti et al. (2004) has estimated metallicities (grey stars in the figures).

As we can see in Fig. 8, by overlaying our distribution of dwarf galaxies on Fig. 4 of Hoyle et al. (2012), we can see that all of our dwarf galaxies are members of the blue dwarf galaxy population. (The Gaussian parameters for the curves are taken from Table 3 in Hoyle et al. (2012).) This is as expected, since the Direct T_e method requires measurements of the emission lines of the galaxies; these emission lines are caused by the UV photons of newly formed stars, indicating a star-forming galaxy and giving the galaxy a blue color.

While the majority of our galaxies follow the positive correlation between color and metallicity, the group of extremely low-metallicity galaxies is clearly separate from the rest. However, when compared to the color curves in Fig. 8, these galaxies occupy the typical range of blue dwarf galaxies, so their colors are not unique. There is no clear separation between the void and wall dwarf galaxies in Fig. 7, indicating that there is little or no large-scale environmental influence on the color-metallicity relation of these galaxies.

5. DISCUSSION

5.1. Large-scale environmental influence

We find no clear distinction between the metallicities of dwarf galaxies in voids and dwarf galaxies in more dense regions. This result agrees with the results of Mouhcine et al. (2007); Nicholls et al. (2014); Kreckel et al. (2015) but disproves our initial hypothesis and contradicts the published results of Pustilnik et al. (2006, 2011b); Pustilnik (2014); Cooper et al. (2008);

Filho et al. (2015); Sánchez Almeida et al. (2016). Deng (2011) also reports a relationship between environment and metallicity. However, he highlights a large difference in metallicity as a function of redshift which correlates with his two samples. It is possible that the dependence he found is actually the result of a systematic dependence on redshift in the metallicity calculation.

Many studies suggest that the metallicity of void galaxies should, on average, be lower than that of galaxies in more dense regions. Mouhcine et al. (2007) and Cooper et al. (2008) both performed statistical studies of this relationship on SDSS DR4, and Deng (2011) repeated this with the DR7 data (only looking at galaxies with a redshift $z > 0.02$). Mouhcine et al. (2007) concluded that the relation between stellar mass and metallicity is much stronger than that between a galaxy’s environment and its metallicity. Cooper et al. (2008) found a more substantial correlation between a galaxy’s environment and its metallicity, but points out that the noise of the different methods used to calculate metallicity is larger than any environment-metallicity relation. Our analysis shows that there is very little difference between the void and wall dwarf galaxies, suggesting that the large-scale environment does not strongly influence the stellar evolution of a galaxy.

There are a few possible explanations as to why there is no difference in the metallicity of void and wall dwarf galaxies. The recycling of the interstellar medium (ISM) of a galaxy can be described by models that lie at two extremes: a “closed box” and an “open box” model. In its simplest form, the closed box model (Talbot & Arnett 1971) describes a galaxy which has no interaction with

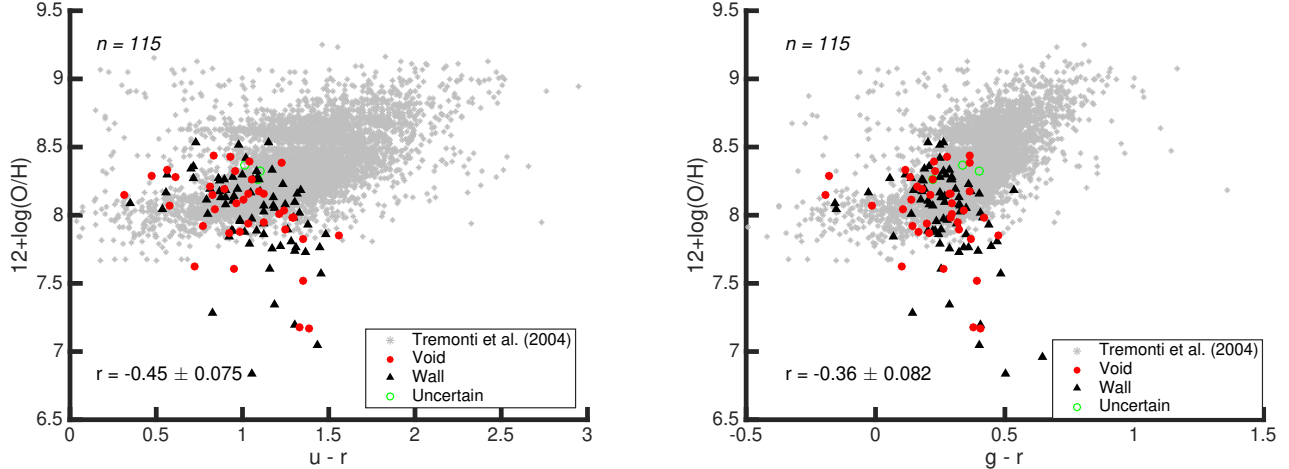


Figure 7. Color ($u-r$ and $g-r$) versus metallicity of the 115 analyzed dwarf galaxies. Error bars have been omitted for clarity. Metallicity is expected to have a positive correlation with color, as older galaxies are expected to have higher metallicities. To place our galaxies in the context of the dwarf galaxy population, we also plot (grey stars) dwarf galaxies ($M_r > -17$) with metallicity estimates by Tremonti et al. (2004). We find no significant difference between the void and wall dwarf galaxies, indicating little to no large-scale environmental influence on the color-metallicity relation.

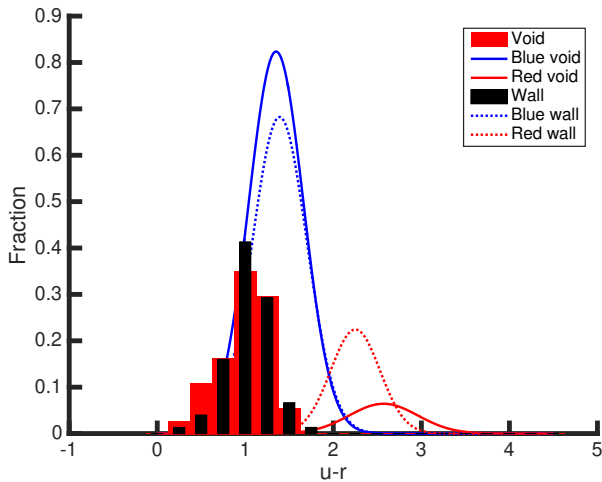


Figure 8. The $u-r$ color distribution of our 115 dwarf galaxies as compared to the color distribution of all SDSS dwarf galaxies as found in Fig. 4 of Hoyle et al. (2012). It is clear that our galaxies are among the bluest dwarf galaxies in SDSS.

its environment — no material enters or leaves the region. A galactic fountain (Shapiro & Field 1976) is a good visualization of the closed box model — any gas expelled during a supernova falls back onto the galaxy. In this model, the gas is very turbulent and thus stays well-mixed throughout the galaxy. Due to the retention of all metals produced by the stars, a galaxy’s metallicity will continue to increase through time (evidence for which was recently shown by Zahid et al. (2012)).

In the open box model (Hartwick 1976), a galaxy’s ISM is regularly influenced by the surrounding environment. Here, pristine gas falls onto the galaxy, providing a constant supply of fresh gas from which to form stars.

In addition, gas expelled in supernovae can be driven from the galaxy. As a result, a galaxy following an open box model could have a metallicity value that evolves very little with time, if it is constantly accreting pristine gas and if it retains very little of the heavy metals its stars generate.

Possible processes that can change the metallicity of a galaxy include:

1. Increases metallicity
 - (a) Supernovae from recent star formation releases metal-rich gas into the ISM
 - (b) Metal-rich gas expelled from an earlier supernova falls back into the galaxy (galactic fountain)
 - (c) Galactic interactions induce a burst of star formation
 - (d) Star formation due to internal secular evolution
2. Decreases metallicity
 - (a) Relatively pristine gas falls onto the galaxy
 - (b) A supernova-driven wind blows metal-rich gas out of the galaxy
 - (c) Interactions with another galaxy strip gas from the galaxy (strangulation, harassment, and/or ram-pressure stripping)

Due to their large-scale environment, void galaxies undergo fewer galactic interactions than wall galaxies. Therefore, these theories dictate that void galaxies more closely follow the closed box model, while wall galaxies

resemble more of an open box. As a result, items 1c and 2c are less relevant for void galaxies, while item 2a is less likely for wall galaxies; this is why the metallicities of void dwarf galaxies are expected to be less than that of wall galaxies. While interactions that the wall galaxies experience may cause more star formation over a given period of time, these collisions may also strip much of the metal-rich gas from dwarf galaxies, causing their metallicities to be similar to that of the void dwarfs.

The void galaxies may be recycling their own gas, since there are relatively fewer interactions to remove the metals released by supernovae. Recently, [McQuinn et al. \(2015\)](#) demonstrated that the isolated dwarf galaxy Leo P has retained significantly more of its metals than dwarf galaxies in more dense regions, particularly the gas-phase metals. Since dwarf galaxies have a smaller gravitational potential than larger galaxies, the supernovae might blow these metal-enriched gases further from the center of the galaxy. Recent simulations by [Melioli et al. \(2015\)](#) on the influence of star formation and supernovae on dwarf galaxy outflows and chemical enrichment appear to support this theory; they find that the metal-rich SN ejecta is thrown far from the galactic plane of dwarf galaxies, even for low SN rates (7×10^{-5} to $7 \times 10^{-4} \text{ yr}^{-1}$). In galaxies in more dense regions, this would increase the opportunity for other galaxies to gather that gas, stripping it from the source galaxy (and thus not allowing it to contribute to the metallicity of the source galaxy). In contrast, in voids, this gas could eventually fall back onto the dwarf galaxies, as there are significantly fewer surrounding galaxies that could strip this gas away.

In addition, void galaxies may also have a more constant supply of pristine gas to support star formation for longer episodes than those galaxies in more dense regions. [Brisbin & Harwit \(2012\)](#) have shown that most star-forming galaxies with $M_* < 2.0 \times 10^{10} M_\odot$ appear to be fed by the infall of pristine or low-metallicity gas. [Moran et al. \(2012\)](#) also found that the lowest-mass galaxies ($\log(M_*) < 10.2 M_\odot$) have a sharp decline in their metallicity at large radii; coupled with a strong correlation to the galaxies' H I masses, they concluded that this indicates newly accreted pristine gas in the galaxies. Since all our dwarf galaxies recently experienced recent star formation, they most likely have recently acquired some quantity of pristine gas. Because void galaxies are more isolated than wall galaxies, their supply is probably more constant, allowing for a more constant rate of star formation throughout their history. In addition, [Moorman et al. \(2016\)](#) has found a slightly higher SFE for void dwarf galaxies. Combined with the likelihood to retain more metals, this might contribute to the similar metallicity distribution in the void and

wall dwarf galaxy populations.

5.2. Comparison to previously published metallicity measurements

To place our metallicity measurements in the context of previous work, we compare our results to the metallicity values measured by [Tremonti et al. \(2004\)](#). While we both use data from the MPA-JHU value-added catalog, [Tremonti et al. \(2004\)](#) employs an empirical method for estimating the metallicity, which is based on calibrated relationships between direct metallicity values and strong-line ratios. The results of this comparison are shown in Figure 9. Unfortunately, the range of metallicity values found by [Tremonti et al. \(2004\)](#) is limited to those galaxies with high metallicities ($12 + \log(\text{O}/\text{H}) > 8.5$), due to the characteristics of their sample and their method; they found less than 2% of their total sample to have metallicities less than 8.5. [Kennicutt et al. \(2003\)](#) shows that methods which make extensive use of the strong emission lines (so-called “strong-line” methods) can overestimate the metallicity abundances by as much as 0.3 dex. A similar comparison is made in [Yin et al. \(2007\)](#), where they too find that the metallicity estimates of [Tremonti et al. \(2004\)](#) are overestimated by 0.34 dex on average. This can be seen quite clearly in Figure 9, as there is no correlation between galaxies with our estimates of $12 + \log(\text{O}/\text{H}) < 8$ and the metallicities measured by [Tremonti et al. \(2004\)](#), since their metallicities are much higher than ours. The formal correlation coefficient between these two data sets is 0.08 ± 0.094 ; the correlation coefficient for those galaxies we measure to have metallicities greater than 7.6 (so excluding the low-metallicity galaxies) is 0.19 ± 0.095 . While this shows a slightly stronger correlation, we realize that the scale over which these metallicities reside is quite small. As a result, any scatter due to the errors in the calculations will result in a bad correlation coefficient, which is what we see. Therefore, by Fig. 9, we can see that there is a reasonable correlation between our metallicity values and those of [Tremonti et al. \(2004\)](#), excluding those galaxies we found to have extremely low metallicity values.

While it is known that there are systematic offsets between different metallicity calculation methods ([Kewley & Ellison 2008](#)), that does not seem to be the case in the relation between our metallicities (measured with the Direct T_e method) and those of [Tremonti et al. \(2004\)](#) (measured with a combination of “strong-line” methods). While the metallicity estimates by [Tremonti et al. \(2004\)](#) are reasonable in the high-metallicity regime, they overestimate the metallicities for low-metallicity galaxies.

5.3. Extreme low-metallicity galaxies

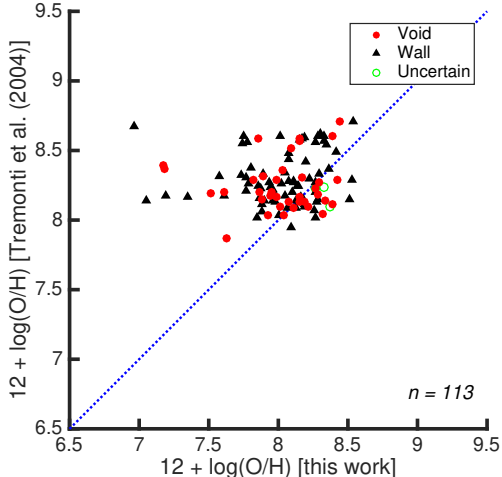


Figure 9. Metallicity ($12 + \log(\text{O}/\text{H})$) comparison between our calculated estimates and those made by Tremonti et al. (2004). Error bars have been omitted for clarity. Excepting the extreme low-metallicity galaxies we found, most galaxies have a reasonable correlation with those already published. It is important to note that the strong-line methods (like those used by Tremonti et al. 2004) are not calibrated for low-metallicity values and are known to overestimate the metallicity by as much as 0.3 dex (Kennicutt et al. 2003). Thus, it is not surprising that oxygen abundances measured using the direct method find lower metallicity, particularly at very low metallicities.

Based on observations of six extremely low-metallicity galaxies found in voids, Pustilnik et al. (2006, 2011b); Pustilnik et al. (2013) infer that there is a fractionally larger population of metal-poor galaxies located in voids than in more dense regions. Of the 115 galaxies we analyze, ten have extremely low gas-phase metallicity values ($12 + \log(\text{O}/\text{H}) < 7.6$); they are highlighted in Table 2. Of these ten galaxies, three are found in voids (roughly 8% of the dwarf void population measured) and seven are located in more dense regions (about 9% of the dwarf wall population measured). These nearly identical population fractions indicate that no special population of extreme metal-poor galaxies exist in the voids. None of these galaxies share the same local environment (none are neighbors to each other). In addition, Fig. 3 shows no evidence to support a special population of extremely metal-poor galaxies in the voids, as extremely metal-poor galaxies are also present in the more dense regions.

We find that these ten extremely metal-poor galaxies are redder and have a lower (s)SFR than the others when looking at the color (Fig. 7) and (specific) star formation rate (Fig. 6) of the 115 analyzed galaxies.

Two of these ten dwarf galaxies have metallicities $12 + \log(\text{O}/\text{H}) < 7.0$, which would make them the most metal-poor galaxies yet discovered. The detection of the temperature-sensitive [O III] $\lambda 4363$ emission line is very weak in each of these galaxies; with such a strong de-

pendence on this line for the calculation of the metallicity, a high-resolution, high quality spectrum is necessary. The flux of this line as calculated from the SDSS DR7 pipeline is larger than the fluxes from the MPA-JHU catalog – for all ten of these extreme low-metallicity galaxies, the average difference between these two sources is 2.2×10^{-17} erg/s/cm². If the SDSS DR7 data had instead been used in this analysis, the metallicity of these ten galaxies would have been even smaller. Further study of these two galaxies in particular is recommended, to confirm these metallicity values and discover why the metallicities are so low.

6. CONCLUSIONS

Using spectroscopic line flux measurements of galaxies in the SDSS DR7 sample available through the MPA-JHU catalog, we estimate the metallicity of dwarf galaxies based on the Direct T_e method. From the 115 galaxies analyzed, there appears to be no large-scale environmental dependence of the metallicity of these galaxies, as the distributions of metallicity values are very similar for those residing in voids and those in more dense regions. Thus, the large-scale (~ 10 Mpc) environment does not appear to strongly influence the chemical evolution of dwarf galaxies.

We examine the relationship between metallicity and other physical characteristics of our dwarf galaxies. In the mass-metallicity relation, our galaxies are at the low-mass extreme; the extreme low metallicity galaxies we found are scattered below this relation. All our dwarf galaxies are at the upper limit in total (s)SFR, and they are on the blue end of the color spectrum. There is no large-scale environmental dependence of the metallicity in any of these categories.

No special population of extremely metal-poor galaxies is found in the voids, as extremely metal-deficient galaxies are found in both voids and walls. A more detailed study of these ten galaxies is recommended, to confirm their metallicity values and discover characteristics shared by the population. As it stands, these ten galaxies include two galaxies which have metallicities $12 + \log(\text{O}/\text{H}) < 7.0$, making them among the lowest metallicity galaxies known.

Although over 800,000 galaxies in SDSS DR7 have spectroscopic observations, only 115 are dwarf galaxies with metal line fluxes necessary to estimate gas-phase oxygen abundances using the Direct T_e method. Unfortunately, this was not enough to re-calibrate any of the more common methods used to calculate metallicity for use on dwarf galaxies. Better data are required to discern the metallicity of a larger selection of dwarf galaxies, from which accurate calibrations can be developed. These estimated ionic abundances can then be compared with predictions of the environmental de-

Table 2. Extreme low-metallicity dwarf galaxies

Index	RA	dec	redshift	$12 + \log\left(\frac{\text{O}}{\text{H}}\right)$	Void/Wall
1873221	09 ^h 35 ^m 53 ^s .48	+29°18'13".46	0.0236	6.84±0.39	Wall
1899071	12 ^h 41 ^m 34 ^s .50	+35°06'34".64	0.0236	6.96±0.45	Wall
1866832	12 ^h 11 ^m 31 ^s .82	+36°51'33".90	0.0243	7.05±0.33	Wall
1899980	11 ^h 34 ^m 59 ^s .61	+35°07'20".26	0.0254	7.17±0.34	Void
839665	08 ^h 09 ^m 53 ^s .51	+29°17'05".04	0.0281	7.18±0.45	Void
1168448	11 ^h 06 ^m 41 ^s .01	+45°19'09".31	0.0220	7.19±0.46	Wall
1986847	13 ^h 00 ^m 00 ^s .39	+30°39'54".52	0.0251	7.28±0.45	Wall
833588	08 ^h 43 ^m 10 ^s .71	+43°08'53".53	0.0245	7.34±0.41	Wall
431383	08 ^h 58 ^m 44 ^s .96	+50°29'58".71	0.0230	7.52±0.61	Void
1322765	14 ^h 15 ^m 05 ^s .59	+36°22'57".75	0.0273	7.57±0.39	Wall

NOTE—Details of the ten extreme low gas-phase metallicity ($12 + \log(\text{O}/\text{H}) < 7.6$) galaxies found. Three of these galaxies are located in voids (about 8% of the void dwarf population measured) and seven are in more dense regions (about 9% of the wall dwarf population measured); thus, there does not seem to be a special population of extreme low-metallicity galaxies in voids. Further study of these galaxies is recommended, to confirm metallicity values and identify any shared characteristics.

pendence of star formation and metallicity from high-resolution hydrodynamic simulations.

Support for this work was provided by NSF grant AST-1410525.

Funding for the SDSS and SDSS-II has been provided by the Alfred P. Sloan Foundation, the Participating Institutions, the National Science Foundation, the U.S. Department of Energy, the National Aeronautics and Space Administration, the Japanese Monbukagakusho, the Max Planck Society, and the Higher Education Funding Council for England. The SDSS Web Site is <http://www.sdss.org/>.

The SDSS is managed by the Astrophysical Research Consortium for the Participating Institutions. The Par-

ticipating Institutions are the American Museum of Natural History, Astrophysical Institute Potsdam, University of Basil, University of Cambridge, Case Western Reserve University, University of Chicago, Drexel University, Fermilab, the Institute for Advanced Study, the Japan Participation Group, Johns Hopkins University, the Joint Institute for Nuclear Astrophysics, the Kavli Institute for Particle Astrophysics and Cosmology, the Korean Scientist Group, the Chinese Academy of Sciences (LAMOST), Los Alamos National Laboratory, the Max-Planck-Institute for Astronomy (MPIA), the Max-Planck-Institute for Astrophysics (MPA), New Mexico State University, Ohio State University, University of Pittsburgh, University of Portsmouth, Princeton University, the United States Naval Observatory, and the University of Washington.

REFERENCES

- Abazajian, K. N., Adelman-McCarthy, J., Agueros, M. A., et al. 2009, *ApJS*, 182, 543
- Ahn, C. P., Alexandroff, R., Allende Prieto, C., et al. 2012, *ApJS*, 203, 21
- Andrews, B. H., & Martini, P. 2013, *ApJ*, 765, 140
- Ann, H. B., Park, C., & Choi, Y.-Y. 2008, *MNRAS*, 389, 86
- Bell, E. F., & de Jong, R. S. 2000, *MNRAS*, 312, 497
- Beygu, B., Kreckel, K., van der Hulst, J. M., et al. 2016, *MNRAS*, 458, 394
- Blanton, M. R., Lin, H., Lupton, R. H., et al. 2003, *AJ*, 125, 2276
- Bond, J. R., Kofman, L., & Pogosyan, D. 1996, *Nature*, 380, 603
- Brinchmann, J., Charlot, S., White, S. D. M., et al. 2004, *MNRAS*, 351, 1151
- Brisbin, D., & Harwit, M. 2012, *ApJ*, 750, 142
- Cen, R. 2011, *ApJ*, 741, 99
- Choi, Y.-Y., Han, D.-H., & Kim, S. S. 2010, *JKAS*, 43, 191
- Cooper, M. C., Tremonti, C. A., Newman, J. A., & Zabludoff, A. I. 2008, *MNRAS*, 390, 245
- Croton, D. J., Farrar, G. R., Norberg, P., et al. 2005, *MNRAS*, 356, 1155
- Cybulski, R., Yun, M. S., Fazio, G. G., & Gutermuth, R. A. 2014, *MNRAS*, 439, 3564
- de Lapparent, V., Geller, M. J., & Huchra, J. P. 1986, *ApJL*, 302, L1
- De Robertis, M., Dufour, R., & Hunt, R. 1987, *JRASC*, 81, 195
- Delahaye, F., & Pinsonneault, M. H. 2006, *ApJ*, 649, 529
- Deng, X.-F. 2011, *AJ*, 141, 162

- Dopita, M. A., Sutherland, R. S., Nicholls, D. C., Kewley, L. J., & Vogt, F. P. 2013, *ApJS*, 208
- Fakhouri, O., & Ma, C.-P. 2009, *MNRAS*, 394, 1825
- Filho, M. E., Sánchez Almeida, J., Muñoz-Tuñón, C., et al. 2015, *ApJ*, 802, 82
- Fukugita, M., Ichikawa, T., Gunn, J. E., et al. 1996, *AJ*, 111, 1748
- Gao, L., & White, S. D. M. 2007, *MNRAS*, 377, L5
- Garnett, D. R. 1992, *AJ*, 103, 1330
- Geha, M., Blanton, M. R., Yan, R., & Tinker, J. L. 2012, *ApJ*, 757, 85
- Goldberg, D. M., Jones, T. D., Hoyle, F., et al. 2005, *ApJ*, 621, 643
- Goldberg, D. M., & Vogeley, M. S. 2004, *ApJ*, 605, 1
- Gottlöber, S., Lokas, E. L., Klypin, A., & Hoffman, Y. 2003, *MNRAS*, 344, 715
- Gregory, S. A., & Thompson, L. A. 1978, *ApJ*, 222, 784
- Grogin, N. A., & Geller, M. J. 2000, *AJ*, 119, 32
- Gunn, J. E., Carr, M., Rockosi, C., et al. 1998, *AJ*, 116, 3040
- Guseva, N., Papaderos, P., Meyer, H., Izotov, Y., & Fricke, K. 2009, *A&A*, 505, 63
- Hartwick, F. D. A. 1976, *ApJ*, 209, 418
- Henry, A., Martin, C. L., Finlator, K., & Dressler, A. 2013, *ApJ*, 769, 148
- Hirschmann, M., De Lucia, G., Wilman, D., et al. 2014, *MNRAS*, 444, 2938
- Hoyle, F., Rojas, R. R., Vogeley, M. S., & Brinkmann, J. 2005, *ApJ*, 620, 618
- Hoyle, F., & Vogeley, M. S. 2002, *ApJ*, 566, 641
- Hoyle, F., Vogeley, M. S., & Pan, D. 2012, *MNRAS*, 426, 3041
- Hughes, T. M., Cortese, L., Boselli, A., Gavazzi, G., & Davies, J. I. 2013, *A&A*, 550, A115
- Izotov, Y., Stasinska, G., Meynet, G., Guseva, N., & Thuan, T. 2006, *A&A*, 448, 955
- Jones, M. G., Papastergis, E., Haynes, M. P., & Giovanelli, R. 2016, *MNRAS*, 457, 4393
- Kennicutt, Jr., R. C., Bresolin, F., & Garnett, D. R. 2003, *ApJ*, 591, 801
- Kereš, D., Katz, N., Weinberg, D. H., & Davé, R. 2005, *MNRAS*, 363, 2
- Kewley, L., & Dopita, M. 2002, *ApJS*, 142, 35
- Kewley, L. J., & Ellison, S. L. 2008, *ApJ*, 681, 1183
- Kirshner, R. P., Oemler, Jr., A., Schechter, P. L., & Shectman, S. A. 1981, *ApJL*, 248, L57
- Kniazev, A. Y., Zijlstra, A. A., Grebel, E. K., et al. 2008, *MNRAS*, 388, 1667
- Kravtsov, A. 2009, in *Astronomical Society of the Pacific Conference Series*, Vol. 419, *Galaxy Evolution: Emerging Insights and Future Challenges*, ed. S. Jogee, I. Marinova, L. Hao, & G. A. Blanc, 283
- Kreckel, K., Croxall, K., Groves, B., van de Weygaert, R., & Pogge, R. W. 2015, *ApJL*, 798, L15
- Kreckel, K., Platen, E., Aragon-Calvo, M., et al. 2012, *AJ*, 144, 16
- Lackner, C. N., Cen, R., Ostriker, J. P., & Joung, M. R. 2012, *MNRAS*, 425, 641
- Lara-Lopez, M., Hopkins, A., Lopez-Sanchez, A., et al. 2013, *MNRAS*, 434, 451
- Lupton, R., Gunn, J. E., Ivezić, Z., Knapp, G. R., & Kent, S. 2001, in *Astronomical Society of the Pacific Conference Series*, Vol. 238, *Astronomical Data Analysis Software and Systems X*, ed. F. R. Harnden, Jr., F. A. Primini, & H. E. Payne, 269
- Mannucci, F., Cresci, G., Maiolino, R., Marconi, A., & Gnerucci, A. 2010, *MNRAS*, 408, 2115
- Marino, R. A., Rosales-Ortega, F. F., Sánchez, S. F., et al. 2013, *A&A*, 559, A114
- McQuinn, K. B. W., Skillman, E. D., Dolphin, A., et al. 2015, *ApJL*, 815, L17
- Melioli, C., Brighenti, F., & D’Ercole, A. 2015, *MNRAS*, 446, 299
- Moorman, C. M., Moreno, J., White, A., et al. 2016, *ArXiv e-prints*, arXiv:1601.04092
- Moorman, C. M., Vogeley, M. S., Hoyle, F., et al. 2015, *ApJ*, 810, 108
- Moran, S. M., Heckman, T. M., Kauffmann, G., et al. 2012, *ApJ*, 745, 66
- Mouhcine, M., Baldry, I., & Bamford, S. 2007, *MNRAS*, 382, 801
- Nicholls, D. C., Jerjen, H., Dopita, M. A., & Basurah, H. 2014, *ApJ*, 780, 88
- Osterbrock, D. E. 1989, *Astrophysics of Gaseous Nebulae and Active Galactic Nuclei* (Mill Valley, CA: University Science Books)
- Pan, D. C., Vogeley, M. S., Hoyle, F., Choi, Y.-Y., & Park, C. 2012, *MNRAS*, 421, 926
- Park, C., Choi, Y.-Y., Vogeley, M. S., et al. 2007, *ApJ*, 658, 898
- Patiri, S. G., Prada, F., Holtzman, J., Klypin, A., & Betancort-Rijo, J. 2006, *MNRAS*, 372, 1710
- Pettini, M., & Pagel, B. E. 2004, *MNRAS*, 348, L59
- Pilyugin, L. S., & Mattsson, L. 2011, *MNRAS*, 412, 1145
- Pilyugin, L. S., & Thuan, T. X. 2007, *ApJ*, 669, 299
- Pilyugin, L. S., Thuan, T. X., & Vilchez, J. M. 2006, *MNRAS*, 367, 1139
- Pustilnik, S., Engels, D., Kniazev, A., et al. 2006, *AstL*, 32, 228
- Pustilnik, S., Martin, J., Tepliakova, A., & Kniazev, A. 2011a, *MNRAS*, 417, 1335
- Pustilnik, S., Tepliakova, A., & Kniazev, A. 2011b, *AstBu*, 66, 255
- Pustilnik, S. A. 2014, *ArXiv e-prints*, arXiv:1412.1316
- Pustilnik, S. A., Martin, J.-M., Lyamina, Y. A., & Kniazev, A. Y. 2013, *MNRAS*, 432, 2224
- Rojas, R. R., Vogeley, M. S., Hoyle, F., & Brinkmann, J. 2004, *ApJ*, 617, 50
- . 2005, *ApJ*, 624, 571
- Saintonge, A. 2007, PhD thesis, Cornell University
- Sánchez Almeida, J., Pérez-Montero, E., Morales-Luis, A. B., et al. 2016, *ApJ*, 819, 110
- Shapiro, P. R., & Field, G. B. 1976, *ApJ*, 205, 762
- Strauss, M. A., Weinberg, D. H., Lupton, R. H., et al. 2002, *AJ*, 124, 1810
- Sutter, P. M., Lavaux, G., Wandelt, B. D., et al. 2014, *MNRAS*, 442, 3127
- Talbot, Jr., R. J., & Arnett, W. D. 1971, *ApJ*, 170, 409
- Tremonti, C. A., Heckman, T. M., Kauffmann, G., et al. 2004, *ApJ*, 613, 898
- van de Weygaert, R., & Platen, E. 2011, *International Journal of Modern Physics Conference Series*, 1, 41
- von Benda-Beckmann, A. M., & Müller, V. 2008, *MNRAS*, 384, 1189
- Yin, S., Liang, Y., Hammer, F., et al. 2007, *A&A*, 462, 535
- Zahid, H. J., Dima, G. I., Kewley, L. J., Erb, D. K., & Davé, R. 2012, *ApJ*, 757, 54

APPENDIX
A. GALAXY DATA

Table A1. Dwarf galaxy properties

Index ^a	RA	dec	redshift	M_r	$12 + \log\left(\frac{O}{H}\right)$	Void/Wall
63713	09 ^h 20 ^m 04 ^s .27	-00°30'08".95	0.0257	-16.73	7.80±0.41	Wall
73537	09 ^h 25 ^m 24 ^s .23	+00°12'40".39	0.0250	-16.94	7.94±0.34	Wall
168874	11 ^h 45 ^m 13 ^s .15	-01°48'17".61	0.0274	-16.99	8.16±0.31	Wall
247831	14 ^h 09 ^m 42 ^s .85	+64°29'36".04	0.0292	-16.93	7.89±0.40	Void
387354	09 ^h 51 ^m 25 ^s .06	+01°55'13".64	0.0249	-16.63	8.14±0.38	Wall
430989	10 ^h 17 ^m 11 ^s .85	+57°55'21".45	0.0267	-16.97	8.02±0.35	Wall
431383	08 ^h 58 ^m 44 ^s .96	+50°29'58".71	0.0230	-16.67	7.52±0.61	Void
434348	09 ^h 51 ^m 21 ^s .20	+57°55'53".26	0.0279	-16.91	8.42±0.32	Wall
449887	08 ^h 55 ^m 48 ^s .98	+03°40'41".03	0.0278	-16.98	8.51±0.34	Wall
458253	11 ^h 05 ^m 46 ^s .58	+04°34'27".44	0.0253	-16.70	8.02±0.32	Wall
466013	13 ^h 02 ^m 49 ^s .19	+65°34'49".30	0.0277	-16.99	8.05±0.02	Wall
470050	07 ^h 38 ^m 29 ^s .12	+30°04'38".00	0.0233	-16.61	8.26±0.52	Uncertain
472641	09 ^h 34 ^m 53 ^s .53	+52°44'20".92	0.0251	-16.84	8.30±0.29	Wall
509426	10 ^h 13 ^m 28 ^s .12	+54°55'44".31	0.0255	-16.85	7.90±0.34	Wall
513306	08 ^h 31 ^m 56 ^s .32	+43°36'12".66	0.0271	-16.97	8.26±0.11	Void
579845	13 ^h 44 ^m 37 ^s .63	-01°15'52".59	0.0253	-16.62	8.19±0.33	Wall
800096	09 ^h 41 ^m 41 ^s .84	+46°59'29".72	0.0254	-16.65	8.13±0.35	Wall
817201	09 ^h 50 ^m 40 ^s .63	+47°57'56".97	0.0247	-16.83	7.87±0.40	Void
833588	08 ^h 43 ^m 10 ^s .71	+43°08'53".53	0.0245	-16.79	7.34±0.41	Wall
836299	10 ^h 33 ^m 01 ^s .14	+54°02'17".91	0.0254	-16.75	8.09±0.04	Wall
839665	08 ^h 09 ^m 53 ^s .51	+29°17'05".04	0.0281	-16.97	7.18±0.45	Void
847573	08 ^h 55 ^m 22 ^s .08	+39°23'10".00	0.0278	-16.91	7.73±0.44	Wall
847639	09 ^h 04 ^m 47 ^s .10	+40°48'29".12	0.0260	-16.84	8.07±0.38	Wall
847908	09 ^h 56 ^m 04 ^s .31	+46°41'40".59	0.0260	-16.89	7.79±0.37	Wall
889704	14 ^h 57 ^m 35 ^s .68	+41°38'16".09	0.0252	-16.80	8.15±0.31	Void
890762	09 ^h 02 ^m 49 ^s .80	+37°15'33".19	0.0243	-16.87	7.88±0.29	Wall
894284	09 ^h 36 ^m 20 ^s .29	+41°50'33".77	0.0242	-16.77	8.27±0.24	Wall
916899	10 ^h 00 ^m 36 ^s .24	+54°20'12".30	0.0249	-16.68	7.89±0.28	Wall
920425	13 ^h 12 ^m 25 ^s .05	+58°25'40".59	0.0276	-16.96	7.93±0.40	Wall
930520	10 ^h 51 ^m 42 ^s .83	+07°17'40".88	0.0232	-16.83	8.05±0.38	Wall
937397	10 ^h 15 ^m 02 ^s .54	+07°48'26".68	0.0283	-16.97	7.98±0.40	Wall
982309	14 ^h 36 ^m 39 ^s .59	+50°14'24".07	0.0258	-16.91	8.21±0.22	Void
983968	13 ^h 57 ^m 58 ^s .56	+51°19'26".33	0.0275	-17.0	8.32±0.35	Void
998736	16 ^h 20 ^m 56 ^s .98	+37°58'44".31	0.0274	-16.99	7.76±0.39	Wall
1011079	15 ^h 08 ^m 31 ^s .64	+52°55'56".61	0.0246	-16.89	7.99±0.35	Void
1064689	11 ^h 11 ^m 23 ^s .73	+45°41'31".69	0.0247	-16.71	8.54±0.34	Wall
1065633	08 ^h 40 ^m 45 ^s .43	+32°03'15".51	0.0258	-16.83	7.84±0.15	Wall
1067677	09 ^h 21 ^m 45 ^s .81	+38°18'09".75	0.0270	-16.91	7.86±0.34	Wall
1093185	08 ^h 49 ^m 36 ^s .32	+54°58'10".48	0.0261	-16.90	8.22±0.24	Wall

Table A1 continued

Table A1 (*continued*)

Index ^a	RA	dec	redshift	M_r	$12 + \log\left(\frac{O}{H}\right)$	Void/Wall
1094082	07 ^h 56 ^m 23 ^s .01	+22°01'15".17	0.0234	-16.97	8.16±0.28	Wall
1096859	08 ^h 23 ^m 32 ^s .78	+27°07'52".78	0.0243	-16.64	7.89±0.13	Wall
1124947	12 ^h 16 ^m 39 ^s .45	+14°15'37".06	0.0234	-16.58	8.01±0.16	Wall
1144404	08 ^h 17 ^m 50 ^s .41	+25°29'21".54	0.0276	-16.90	8.19±0.37	Wall
1162831	13 ^h 48 ^m 36 ^s .87	+48°52'58".22	0.0257	-16.79	8.03±0.40	Void
1168448	11 ^h 06 ^m 41 ^s .01	+45°19'09".31	0.0220	-16.39	7.19±0.46	Wall
1168506	11 ^h 17 ^m 33 ^s .06	+45°40'20".76	0.0242	-16.98	7.61±0.28	Wall
1187796	16 ^h 20 ^m 01 ^s .12	+37°13'01".23	0.0281	-16.92	8.11±0.32	Wall
1197981	14 ^h 32 ^m 02 ^s .84	+51°52'52".15	0.0256	-16.70	8.15±0.03	Void
1204380	12 ^h 04 ^m 47 ^s .19	+47°14'04".80	0.0242	-16.87	8.07±0.38	Wall
1209653	16 ^h 15 ^m 47 ^s .10	+28°03'42".95	0.0250	-16.74	7.85±0.32	Void
1212364	16 ^h 16 ^m 38 ^s .89	+29°03'32".45	0.0249	-16.55	8.16±0.22	Void
1223625	13 ^h 08 ^m 21 ^s .42	+11°30'55".02	0.0250	-16.92	8.27±0.24	Wall
1227992	14 ^h 19 ^m 14 ^s .09	+39°57'29".89	0.0255	-16.79	7.96±0.40	Wall
1228962	11 ^h 05 ^m 51 ^s .18	+42°58'09".23	0.0215	-16.88	8.29±0.22	Wall
1231835	11 ^h 59 ^m 08 ^s .00	+44°45'11".77	0.0243	-16.97	8.42±0.36	Void
1238985	11 ^h 57 ^m 26 ^s .81	+45°58'10".61	0.0239	-16.86	8.26±0.14	Wall
1240788	12 ^h 47 ^m 38 ^s .62	+43°31'56".16	0.0251	-16.83	8.13±0.28	Wall
1243238	14 ^h 46 ^m 11 ^s .91	+38°04'52".81	0.0254	-16.66	7.95±0.26	Void
1251819	14 ^h 25 ^m 37 ^s .89	+41°28'04".85	0.0259	-16.80	7.78±0.35	Wall
1255631	11 ^h 55 ^m 23 ^s .95	+11°55'51".11	0.0223	-16.35	8.44±0.39	Void
1262505	13 ^h 30 ^m 48 ^s .44	+12°16'28".10	0.0256	-16.72	8.04±0.07	Void
1265371	13 ^h 12 ^m 35 ^s .15	+12°57'43".36	0.0257	-16.82	8.29±0.04	Void
1265467	13 ^h 29 ^m 18 ^s .76	+12°39'36".86	0.0249	-16.65	8.27±0.38	Wall
1274994	12 ^h 11 ^m 07 ^s .57	+42°04'15".44	0.0228	-16.62	8.10±0.35	Wall
1292068	12 ^h 19 ^m 19 ^s .39	+41°32'17".88	0.0227	-16.70	8.33±0.40	Wall
1294650	15 ^h 13 ^m 58 ^s .18	+33°08'23".20	0.0228	-16.56	8.11±0.22	Void
1297990	14 ^h 20 ^m 11 ^s .80	+38°48'13".49	0.0273	-16.84	7.86±0.42	Wall
1322765	14 ^h 15 ^m 05 ^s .59	+36°22'57".75	0.0273	-16.87	7.57±0.39	Wall
1342776	13 ^h 56 ^m 59 ^s .76	+09°55'49".99	0.0242	-16.91	7.92±0.30	Void
1346719	14 ^h 07 ^m 04 ^s .18	+06°36'16".33	0.0252	-16.82	8.15±0.33	Void
1358827	15 ^h 04 ^m 01 ^s .93	+08°33'09".73	0.0274	-16.99	8.39±0.31	Void
1366354	14 ^h 16 ^m 19 ^s .46	+07°15'29".53	0.0288	-16.94	7.88±0.30	Void
1378430	14 ^h 02 ^m 44 ^s .46	+50°24'47".37	0.0265	-16.93	8.01±0.31	Void
1381082	15 ^h 37 ^m 21 ^s .38	+41°53'53".93	0.0237	-16.67	7.61±0.16	Void
1416109	12 ^h 42 ^m 19 ^s .03	+14°06'29".12	0.0266	-16.89	8.09±0.31	Void
1417239	12 ^h 59 ^m 23 ^s .52	+15°21'37".76	0.0255	-16.81	7.82±0.39	Void
1421138	15 ^h 11 ^m 00 ^s .82	+11°20'24".26	0.0275	-16.98	8.07±0.04	Void
1453971	14 ^h 29 ^m 32 ^s .67	+33°30'40".47	0.0267	-16.97	8.28±0.08	Wall
1702683	07 ^h 52 ^m 12 ^s .03	+46°23'39".91	0.0222	-16.37	8.37±0.30	Uncertain
1775952	07 ^h 30 ^m 03 ^s .58	+43°22'45".16	0.0264	-16.88	8.32±0.37	Uncertain
1785328	08 ^h 00 ^m 41 ^s .21	+53°38'23".53	0.0226	-16.94	7.62±0.35	Void
1843211	10 ^h 02 ^m 41 ^s .40	+32°59'40".09	0.0292	-16.96	7.94±0.09	Void

Table A1 *continued*

Table A1 (*continued*)

Index ^a	RA	dec	redshift	M_r	$12 + \log \left(\frac{O}{H} \right)$	Void/Wall
1850512	10 ^h 55 ^m 15 ^s .97	+37°25'42".61	0.0252	-16.88	7.98±0.38	Wall
1855301	09 ^h 01 ^m 58 ^s .05	+28°58'16".79	0.0262	-16.81	7.77±0.44	Wall
1858237	10 ^h 23 ^m 46 ^s .09	+37°06'38".04	0.0261	-16.90	8.19±0.09	Wall
1866832	12 ^h 11 ^m 31 ^s .82	+36°51'33".90	0.0243	-16.72	7.05±0.33	Wall
1867958	12 ^h 05 ^m 09 ^s .66	+37°16'13".20	0.0226	-16.80	8.18±0.20	Wall
1869724	11 ^h 10 ^m 02 ^s .63	+36°56'04".93	0.0275	-16.98	8.34±0.26	Void
1873221	09 ^h 35 ^m 53 ^s .48	+29°18'13".46	0.0236	-16.61	6.84±0.39	Wall
1876674	08 ^h 20 ^m 31 ^s .61	+21°43'28".81	0.0257	-16.96	8.36±0.21	Wall
1894472	10 ^h 30 ^m 47 ^s .70	+32°15'02".11	0.0215	-16.84	7.75±0.39	Wall
1897348	13 ^h 47 ^m 02 ^s .05	+32°32'59".51	0.0252	-16.64	8.27±0.19	Wall
1899071	12 ^h 41 ^m 34 ^s .50	+35°06'34".64	0.0236	-16.91	6.96±0.45	Wall
1899980	11 ^h 34 ^m 59 ^s .61	+35°07'20".26	0.0254	-16.87	7.17±0.34	Void
1907555	15 ^h 54 ^m 23 ^s .83	+21°34'56".45	0.0274	-16.89	8.39±0.33	Void
1910757	13 ^h 56 ^m 31 ^s .57	+32°50'45".53	0.0273	-16.87	8.34±0.13	Wall
1921758	13 ^h 12 ^m 19 ^s .04	+34°02'01".10	0.0233	-16.54	7.74±0.44	Wall
1928039	11 ^h 19 ^m 59 ^s .99	+34°38'00".30	0.0249	-16.66	8.28±0.12	Wall
1941725	13 ^h 03 ^m 41 ^s .90	+33°09'34".00	0.0240	-16.93	8.33±0.25	Wall
1945788	11 ^h 51 ^m 49 ^s .13	+31°30'14".56	0.0286	-16.92	8.19±0.20	Wall
1970891	13 ^h 35 ^m 16 ^s .22	+28°28'59".75	0.0264	-16.82	8.07±0.16	Wall
1986847	13 ^h 00 ^m 00 ^s .39	+30°39'54".52	0.0251	-16.96	7.28±0.45	Wall
1987036	13 ^h 29 ^m 56 ^s .56	+29°46'19".41	0.0260	-16.89	8.08±0.32	Wall
1992337	15 ^h 58 ^m 34 ^s .00	+16°44'33".12	0.0261	-16.90	8.28±0.26	Void
2243244	12 ^h 22 ^m 15 ^s .32	+28°18'53".10	0.0278	-16.94	7.96±0.22	Wall
2302977	13 ^h 54 ^m 01 ^s .01	+20°30'34".85	0.0269	-16.93	8.17±0.07	Wall
2322803	11 ^h 52 ^m 32 ^s .75	+25°02'35".52	0.028	-16.89	8.13±0.36	Wall
2328013	11 ^h 16 ^m 12 ^s .04	+18°26'25".49	0.0249	-16.77	7.99±0.31	Void
2330295	11 ^h 19 ^m 10 ^s .25	+19°13'04".13	0.0250	-16.87	8.19±0.17	Void
2348655	10 ^h 10 ^m 28 ^s .77	+16°28'13".08	0.0281	-16.89	8.53±0.27	Wall
2352332	10 ^h 59 ^m 21 ^s .21	+19°37'36".28	0.0270	-16.95	8.17±0.33	Wall
2392348	11 ^h 06 ^m 19 ^s .25	+15°32'27".92	0.0271	-16.84	8.17±0.29	Void
2483080	09 ^h 49 ^m 41 ^s .83	+15°24'19".58	0.0262	-16.83	8.11±0.14	Wall
2494742	09 ^h 48 ^m 52 ^s .81	+14°31'38".98	0.0268	-16.97	8.28±0.38	Wall
2496108	10 ^h 11 ^m 16 ^s .61	+16°00'20".04	0.0267	-16.93	7.88±0.13	Wall

NOTE—List of the 115 dwarf galaxies analyzed from SDSS DR7. The flux values for all required emission lines can be found in the MPA-JHU value-added catalog. Metallicity values are calculated using the Direct T_e method, with error estimates via a Monte Carlo method. The void catalog of [Pan et al. \(2012\)](#) is used to classify the galaxies as either Void or Wall. If a galaxy is located too close to the boundary of the SDSS survey to identify whether or not it is inside a void, it is labeled as Uncertain.

^aKIAS-VAGC galaxy index number